Supplement of Atmos. Chem. Phys., 19, 6107–6123, 2019
https://doi.org/10.5194/acp-19-6107-2019-supplement

Atmospheric Chemistry and Physics
Open Access
EGU

Supplement of

Heterogeneous sulfate aerosol formation mechanisms during wintertime Chinese haze events: air quality model assessment using observations of sulfate oxygen isotopes in Beijing

Jingyuan Shao et al.

Correspondence to: Becky Alexander (beckya@uw.edu), Lin Zhang (zhanglg@pku.edu.cn) and Zhouqing Xie (zqxie@ustc.edu.cn)

Text S1. Calculation of $\Delta^{17}O(SO_4^{2-})$ in the model

The oxygen isotopic composition of sulfate ($\Delta^{17}O(SO_4^{2-})$) in the model is calculated as follows:

$$\Delta^{17}O\left({SO_4}^{2-}\right) = \frac{C_{\text{cloud},H_2O_2} \times 0.7 + C_{\text{cloud},O_3} \times 9.75 + C_{\text{het},H_2O_2} \times 0.7 + C_{\text{het},O_3} \times 9.75}{C_{\text{gas}} + C_{\text{cloud}} + C_{\text{het}} + C_{\text{primary}}}$$

where C_{gas}, C_{cloud}, C_{het}, C_{primary} respectively represents sulfate concentration from gas-phase oxidation of SO_2, aqueous phase oxidation of S(IV) in clouds, heterogeneous oxidation of SO_2 on aerosol surfaces, and primary sulfate. The assumed $\Delta^{17}O(SO_4^{2-})$ value for each sulfate production pathway is summarized in Table S1.

In contrast to previous studies (e.g., He et al., 2017), we assume that the terminal oxygen atom is transferred to S(IV) during oxidation based on Liu et al. (2001), leading to higher $\Delta^{17}O(SO_4^{2-})$ values than those when assuming all three oxygen atoms of ozone are equally likely to be transferred to the product sulfate.

Table S1. $\Delta^{17}O(SO_4^{2-})$ value for each sulfate production pathway used in the GEOS-Chem model[1]

Sulfate formation pathway		$\Delta^{17}O(SO_4^{2-})$ ‰
Gas	SO_2+OH	0
In Cloud	S(IV)+H_2O_2	0.7
	S(IV)+O_3	9.75[a]
	S(IV)+TMI	0
On aerosol surface (Heterogeneous)	S(IV)+H_2O_2	0.7
	S(IV)+O_3	9.75
	S(IV)+TMI	0
	S(IV)+NO_2	0
Primary sulfate		0

[1] $\Delta^{17}O(SO_4^{2-})$ values are based on results from Savarino et al. (2000) and Liu et al (2001) and assuming $\Delta^{17}O(O_3)$ = 26‰ (Vicars et al., 2014) and $\Delta^{17}O(H_2O_2)$ = 1.4‰ (Savarino and Thiemens, 1999).

Text S2. Influence of aerosol pH on reaction probability and sulfate production rate

Figure S1 shows the calculated reaction probability (γ, Section 2) and sulfate production rate (R) as a function of aerosol pH for the four heterogeneous sulfate production mechanisms implemented into the model (TMI, O_3, H_2O_2 and NO_2) plus two additional pathways, heterogeneous S(IV) oxidation by HOBr and O_2 on acidic microdroplets as proposed by Hung and Hoffmann (2015). Concentrations used in the calculations shown in Figure S1 represent the HPP conditions: $[SO_2(g)]$ = 20 ppb, $[NO_2(g)]$ = 85 ppb, $[O_3(g)]$ = 11 ppb, $[H_2O_2(g)]$ = 0.3 ppb, [HOBr(g)] = 0.1 ppt, total soluble Fe and Mn are estimated to 10 and 20 ng m^{-3}. Concentrations of H_2O_2 is from Ye et al., (2018) and HOBr is from the standard model simulation, and all others are from observations. The mass accommodation coefficients (α in Eq. (3) in the main text) for SO_2, NO_2, O_3, H_2O_2, and HOBr are 0.23, 2×10^{-4} (Jacob, 2000), 2×10^{-3} (Jacob, 2000), 0.11, and 0.6 (Chen et al., 2016), respectively. Aerosol radius (a in Eq. (1)) and total aerosol surface area (A in Eq. (1)) depend on the type of aerosol. Here we use a =1.5×10^{-5}cm (Cheng, et al., 2016) and A =l2×10^{-5} cm^2 cm^{-3}.

As shown in Figure S1, the calculated reaction probabilities (γ) and sulfate production rates (R) are strongly pH dependent for the different sulfate formation pathways, with the exception of the H_2O_2 pathway. The calculated γ for H_2O_2 oxidation is on the order of 10^{-4} for all aerosol pH values. The lack of pH dependence for S(IV) oxidation by H_2O_2 is due to the competing effects of increases in the pseudo-first order reaction rate constant with $[H^+]$ (the reaction is acid catalyzed) and decreasing SO_2 solubility with decreasing pH. The reaction probabilities and sulfate production rates for O_3 and NO_2 pathways increase with increasing pH because of the increase in the effective Henry's law constant of SO_2 with pH, and are limited by mass transport across the air water interface at high pH values (pH > 7). TMI-catalyzed oxidation plays an important role when pH < 4 due to the increased solubility of Fe and Mn at low pH. Heterogeneous sulfate production rates calculated as first order in SO_2 or oxidant concentrations result in similar values when aerosol pH < 6, and are limited by the mass transport across the

air-water interface at higher pH values. Calculated γ ranges from 8×10^{-6}–7×10^{-4} over all aerosol pH values, consistent with the γ values used in previous studies (Cheng et al., 2016; Zheng et al., 2015). Figure S1 also shows calculated $\Delta^{17}O(SO_4^{2-})$ for sulfate produced via heterogeneous production pathways. Calculated heterogeneous $\Delta^{17}O(SO_4^{2-})$ is lower than 0.1‰ when pH < 4, is about 0.6‰ when pH is between 3 and 5, and increases rapidly to 4.5‰ for pH of 5-7.

The reaction probability γ for the HOBr pathway is limited by mass transfer when pH > 5 due to the large aqueous-phase rate-coefficient for this reaction. Although the γ values for heterogeneous oxidation by HOBr are high (on the order of 10^{-1} as shown in Figure S1), the sulfate production rate is relatively low due to low HOBr concentrations (0.1 ppt) in the model. Chen et al. (2017) showed that HOBr concentrations were likely underestimated in GEOS-Chem; however, HOBr observations in China are not available for comparison with model results shown here. Due to the estimated low reaction rate for heterogeneous sulfate production via oxidation by HOBr and the lack of relevant observational constraints, we do not further consider this reaction pathway in this study. We note that this should be revisited in the future when observational constraints on HOBr abundance become available.

The heterogeneous sulfate production rate for SO_2 oxidation by O_2 on acidic microdroplets is very large due to calculated high γ values (resulting from the large aqueous-phase rate constant in Hung and Hoffman (2015)) and SO_2 concentrations (Figure S1). Implementation of this heterogeneous sulfate formation pathway into GEOS-Chem results in 95% of total, global, tropospheric sulfate formation occurring via this pathway (figure not shown), even though it only occurs in the model when calculated aerosol pH is lower than 3. This result seems highly unrealistic, and thus we do not consider it further here.

Text S3 Comparison of Observed and Modeled Seasonal Mean Mn and Fe

The parameterization of TMI-catalyzed S(IV) oxidation in clouds in GEOS-Chem is described in Alexander et al., (2009). The natural source of Fe ($[Fe]_{nat}$) and Mn ($[Mn]_{nat}$) from mineral dust are scaled to total dust mass. $[Fe]_{nat}$ is 3.5% of total dust mass and $[Mn]_{nat}$ is a factor of 50 lower than $[Fe]_{nat}$ (Alexander et al., 2009). The anthropogenic source of Fe ($[Fe]_{ant}$) and Mn ($[Mn]_{ant}$) from coal combustion are scaled to the abundance of primary anthropogenic sulfate due to their common source and atmospheric lifetime $[Mn]_{ant}$ is 1/300 of primary sulfate concentration and $[Fe]_{ant}$ is 10 times that of $[Mn]_{ant}$ as described in Alexander et al. (2009). Figure S4 show the distribution of simulated $[Fe]_{nat}$ and $[Fe]_{ant}$ during the entire model simulation period. Table S2 compares autumn-winter mean modeled Mn and Fe with the observations at several sites in east Asia, including 3 sites in the North China Plain(NCP) region (Beijing, Tianjin and Shijiazhuang), 2 sites in the Sichuan Basin (Chengdu and Chongqing), and Lanzhou and Seoul which are the upwind and downwind of Beijing, respectively. The model tends to underestimate both Fe and Mn at the NCP sites by a factor of 0.25-0.72. Model comparison with observations in the Sichuan Basin shows good agreement on Mn concentration (within 20% for both Chongqing and Chengdu), with model calculations overestimating the observations of Fe concentrations. For sites in Lanzhou (northwest of Beijing, upwind) and Seoul (southeast of Beijing, downwind), model comparison with observations indicates good agreement on Fe (within 5%), and underestimates Mn by 60%. The model underestimates Fe and Mn in the NCP region and overestimates in Sichuan Basin. These discrepancies highlight the limitations of our approach applying a global-scale factor of $[SO4]_{primary}/[Mn]_{ant}$ and $[dust]/[Fe]_{nat}$, as regionally varying emissions control technologies and mass fraction of Fe in dust may impact the relative emission rates.

However, sulfate formation by the TMI-catalyzed oxidation pathway is influenced by soluble Fe^{3+} and Mn^{2+} concentrations, as opposed to total Fe and Mn. Previous studies suggest that the solubility of Fe and Mn ranges from 0.03 to 54% and 1.2 to 97%, respectively. The solubility of metals is influenced by several factors such as the natural

versus anthropogenic origin of samples (A.R. Baker et al., 2006; K.V. Desboeufs et al., 2005; K.V. Desboeufs et al., 2001; Spokes et al., 1994; A. Ito1 and Y. Feng, 2010; P.Y. Chuang et al., 2005; Solmon et al., 2009), acidity, and sunlight. In this study, we assume a solubility of 10% for $[Fe]_{ant}$, 0.45% for $[Fe]_{nat}$, 50% for $[Mn]_{ant}$, and 5% for $[Mn]_{nat}$ in cloud water. The modeled soluble Fe^{3+} and Mn^{2+} concentration is shown in Table S3. After modification, the average modeled concentration of soluble Fe(III) in cloud water during our study period is 2.9±1.8 μM and Mn(II) is 1.3±0.7 μM, which is consistent with estimates (He et al., 2018) and observations (Shen et al., 2012; Guo et al., 2012). A sensitivity study is performed based on Run_TMI but with the higher solubility of Fe and Mn as Alexander et al. (2009): the solubility of 1% of $[Fe]_{nat}$ and 50% for $[Mn]_{nat}$ in cloud water. The modeled soluble Fe(III) and Mn(II) concentration reaches 20μM and 10 μM during HPP, up to a factor of 5 higher than the observations. The simulated sulfate concentration is also overestimated the observation by around 100% during HPP in Beijing.

Table S2. Comparison of observed and modeled autumn and winter mean Mn and Fe concentrations (ng m^{-3}) from several East Asian locations.

Location	Fe (Mn) observation (ng m^{-3})	Fe (Mn) model (ng m^{-3})	Fe (Mn) Model/observation	Reference
Beijing	1800 (90)	835 (22.7)	0.46 (0.25)	Zhao et al. (2013)
Tianjin	1980 (120)	1239 (36.2)	0.72 (0.30)	
Shijiazhuang	2250 (150)	1615 (44.3)	0.63 (0.30)	
Chengdu	875 (38)	1245.7 (34.1)	1.42 (0.90)	Wang et al. (2018)
Chongqing	502.5 (36.5)	1226.0 (39.7)	2.4 (1.09)	
Lanzhou	1534 (59)	1456.9 (33.0)	0.95 (0.56)	Wang et al. (2016)
Seoul	227 (21)	219.8 (6.1)	0.97 (0.30)	Park et al. (2018)

Table S3. Comparison of observed and modeled soluble Mn(II) and Fe(III) concentrations (μM).

	This study Range (monthly mean)	Beijing (He et al., 2018)	Mt. Tai[a] (Shen et al., 2012)	Mt. Tai (Guo et al., 2012)
Fe(III)	0.4-11.2 (2.9±2.7)	0.6-6.1 (2.6±1.8)	0.8-7.4	2.6
Mn(II)	0.4-4.8 (1.3±0.9)	1	0.4-1.7	1.2

[a]Mt. Tai is located in central Shandong province at the eastern edge of the NCP region.

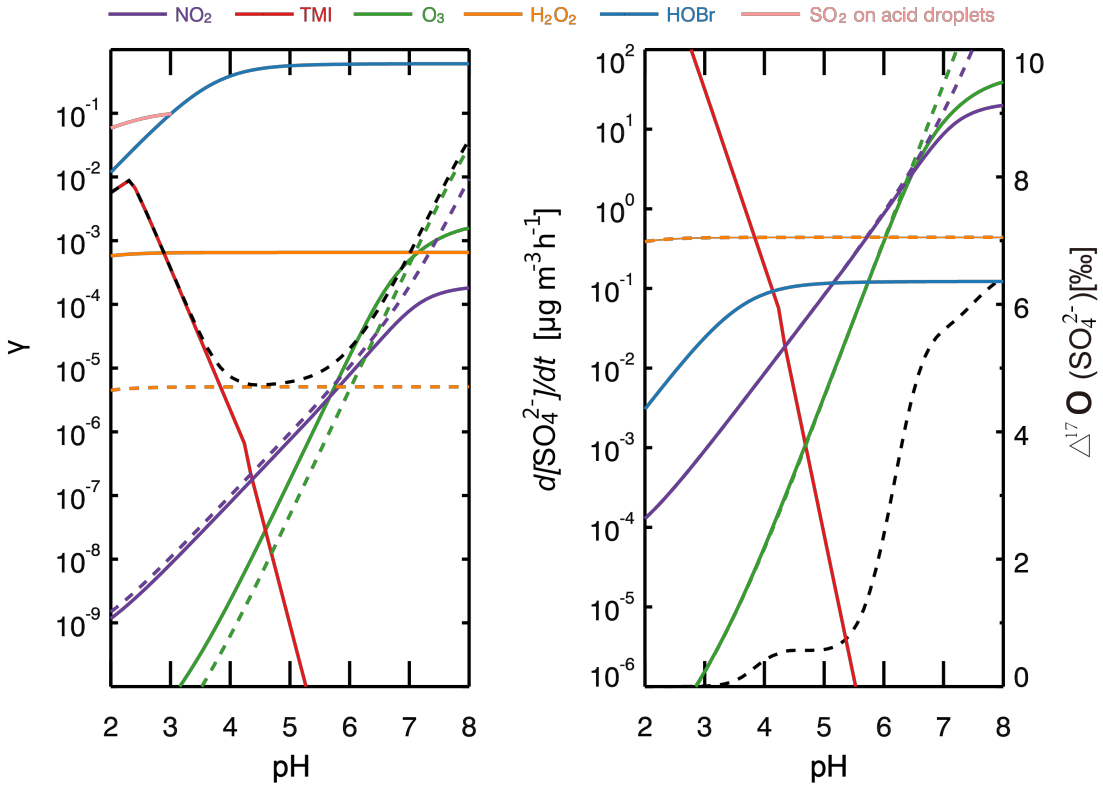

Figure S1. The dependence of reaction probability γ (left) and sulfate production rates (μg m^{-3} h^{-1}) (right) on aerosol pH for different heterogeneous sulfate formation pathways, including NO_2 (purple), TMI (red), O_3 (green), H_2O_2 (orange), HOBr (blue), and SO_2 on acid droplets (pink). The sulfate production rate on acid droplets is not shown on the figure on the right because it is off scale. The solid lines are calculated as first order in the oxidant, and the dashed lines are calculated as first order in SO_2. The black dashed line on the left represents the sum of TMI, O_3, H_2O_2 and NO_2. The black dashed line on the right represents the calculated $\Delta^{17}O(SO_4^{2-})$ value for the four reactions of TMI, O_3, H_2O_2 and NO_2.

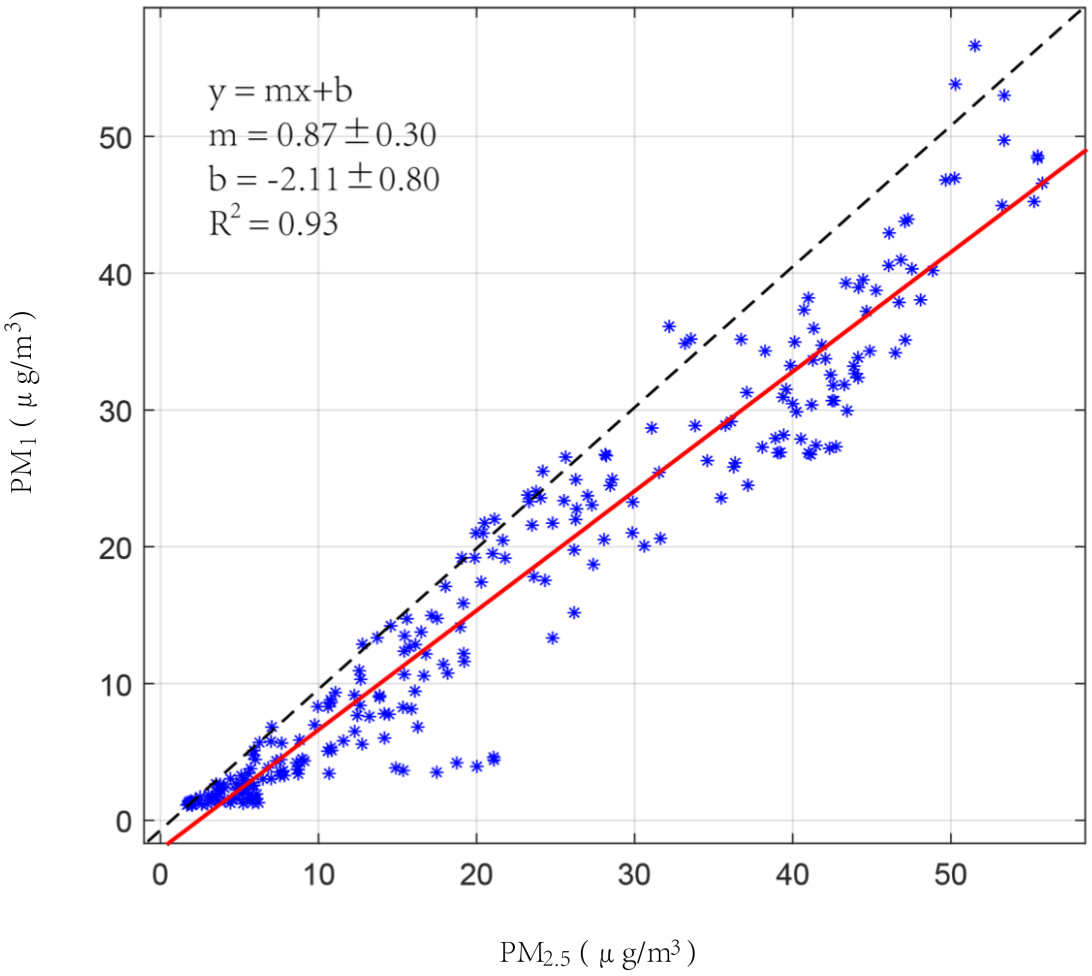

145

Figure S2. The relationship between sulfate concentrations in $PM_{2.5}$ and PM_1 measured in Beijing.

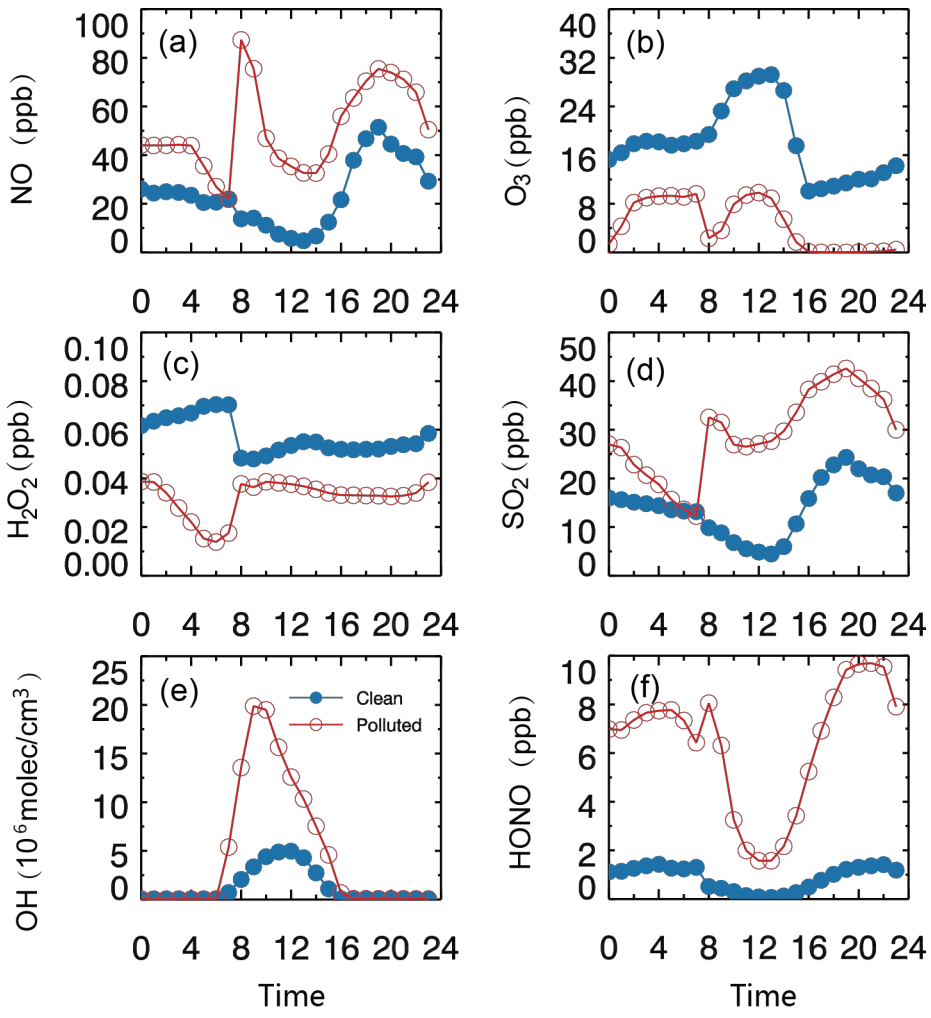

Figure S3. Modeled diurnal cycles of surface NO, O_3, H_2O_2, SO_2, HONO, and OH abundances in Beijing. The red lines denote averages for heavy polluted periods and the blue lines denote averages for clean periods as defined in the text.

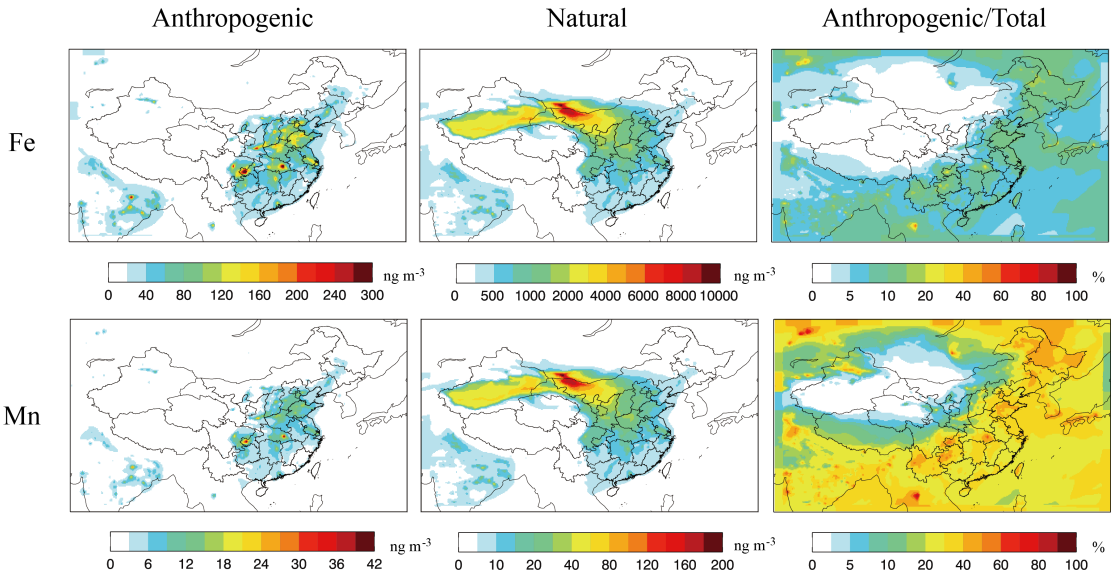

Figure S4. Modeled Anthropogenic and Natural Fe and Mn (ng m^{-3}) at the surface, along with the anthropogenic/total Fe and Mn concentration percentages.

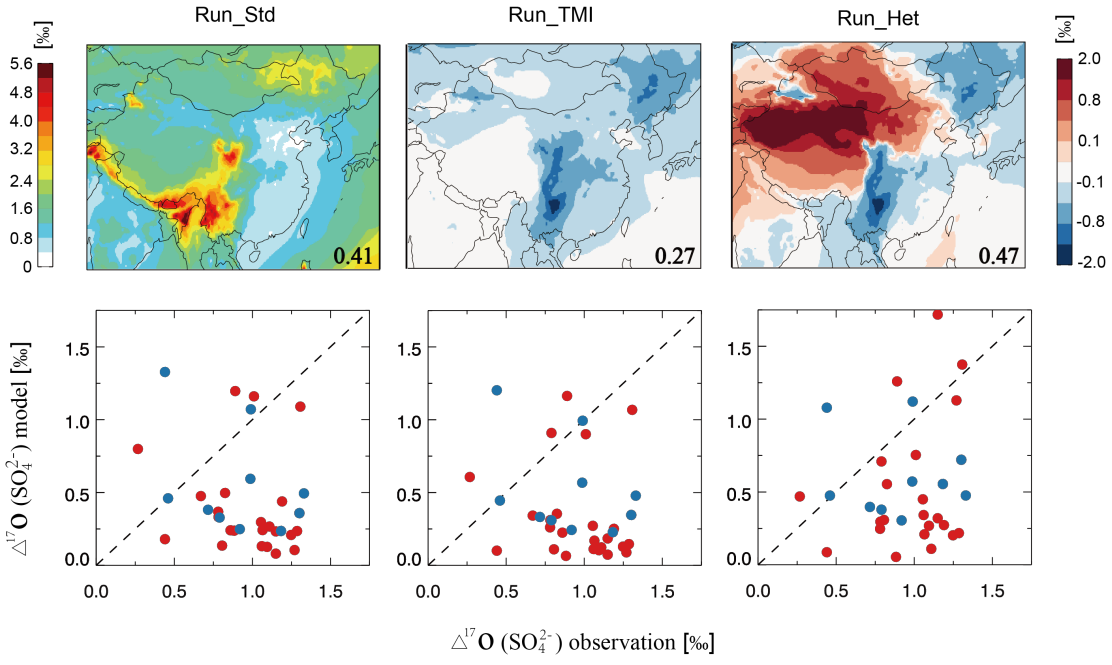

Figure S5. Modeled $\Delta^{17}O(SO_4^{2-})$ and comparisons with observations in Beijing. The top panels show modeled spatial distribution of $\Delta^{17}O(SO_4^{2-})$ over Asia averaged over the measurement period. The top left panel shows simulated $\Delta^{17}O(SO_4^{2-})$ in Run_Std; the middle and right panels show differences relative to Run_Std in Run_TMI and Run_Het, respectively. Numbers in inset are simulated mean $\Delta^{17}O(SO_4^{2-})$ values (‰) in Beijing averaged over the entire collection period. The bottom panels show observed vs. modeled $\Delta^{17}O(SO_4^{2-})$ in Beijing in Run_Std (left), Run_TMI (middle), and Run_Het (right) separated for heavy pollution (HPP; red circles) and clean (CP; blue circles) periods.

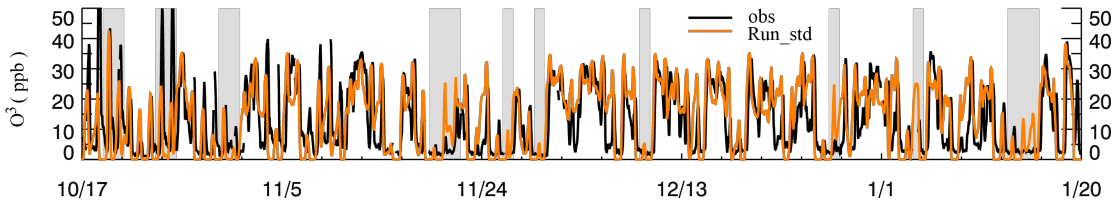

Figure S6. Time series of O_3 at the surface in Beijing during the study period of 17 October 2014 – 20 January 2015. Hourly O_3 observations (black line) are compared with model results from Run_Std (orange line). The gray shaded bars represent 10 heavy pollution periods (HPP) as defined in the text.

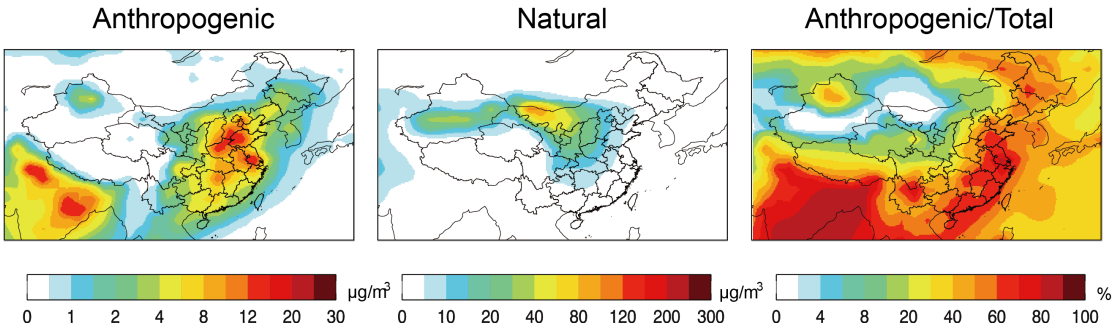

Figure S7. Modeled anthropogenic and natural dust (μg m^{-3}) at the surface, along with the percentage contribution of anthropogenic dust to total dust concentration.

References

Baker, A. R., Jickells, T. D., Witt, M., and Linge, K. L.: Trends in the solubility of iron, aluminium, manganese and phosphorus in aerosol collected over the Atlantic Ocean, Marine Chemistry, 98, 43-58, doi:10.1016/j.marchem.2005.06.004, 2006.

Chuang, P. Y., Duvall, R. M., Shafer, M. M., and Schauer, J. J.: The origin of water soluble particulate iron in the Asian atmospheric outflow, Geophys. Res. Lett., 32,07813-07817, doi:10.1029/2004gl021946, 2005.

Desboeufs, K. V., Losno, R., and Colin, J. L.: Factors influencing aerosol solubility during cloud processes, Atmos. Environ., 35, 3529-3537, doi: 10.1016/s1352-2310(00)00472-6, 2001.

Desboeufs, K. V., Sofikitis, A., Losno, R., Colin, J. L., and Ausset, P.: Dissolution and solubility of trace metals from natural and anthropogenic aerosol particulate matter, Chemosphere, 58, 195-203, doi:10.1016/j.chemosphere.2004.02.025, 2005.

Guo, J., Wang, Y., Shen, X., Wang, Z., Lee, T., Wang, X., Li, P., Sun, M., Collett, J. L., Wang, W., and Wang, T.: Characterization of cloud water chemistry at Mount Tai, China: Seasonal variation, anthropogenic impact, and cloud processing, Atmos. Environ., 60, 467-476, doi:10.1016/j.atmosenv.2012.07.016, 2012.

He, P., Alexander, B., Geng, L., Chi, X., Fan, S., Zhan, H., Kang, H., Zheng, G., Cheng, Y., Su, H., Liu, C., and Xie, Z.: Isotopic constraints on heterogeneous sulfate production in Beijing haze, Atmos. Chem. Phys., 18, 5515-5528, doi:10.5194/acp-18-5515-2018, 2018.

Ito, A., and Feng, Y.: Role of dust alkalinity in acid mobilization of iron, Atmos. Chem. Phys., 10, 9237-9250, doi:10.5194/acp-10-9237-2010, 2010.

Liu, Q., L. M. Schuerter, C. E. Muller, S. Aloisio, J. S. Francisco, and D. W. Margerum (2001), Kinetics and mechanisms of aqueous ozone reactions with bromine, sulfite, hydrogen sulfite, iodide, and nitrite ions, Inorg. Chem., 40, 4436-4442.

Shen, X. H., Lee, T. Y., Guo, J., Wang, X. F., Li, P. H., Xu, P. J., Wang, Y., Ren, Y., Wang, W., Wang, T., Li, Y., Cam, S. A., and Collett, J. L.: Aqueous phase sulfate production in clouds in eastern China, Atmos. Environ., 62, 502-511, doi:10.1016/j.atmosenv.2012.07.079, 2012.

Vicars, W. and J. Savarino . "Quantitative constraints on the ^{17}O-excess (Δ^{17}O) signature of surface ozone: Ambient measurements from 50°N to 50°S using the nitrite-coated filter technique." Geochem. Cosmochem. Acta 135: 270-287, 2014.

Park, S.-M., Song, I.-H., Park, J. S., Oh, J., Moon, K. J., Shin, H. J., Ahn, J. Y., Lee, M.-D., Kim, J., and Lee, G.: Variation of $PM_{2.5}$ Chemical Compositions and their Contributions to Light Extinction in Seoul, Aerosol and Air Quality Research, 18, 2220-2229, doi:10.4209/aaqr.2017.10.0369, 2018.

Savarino, J. and M. H. Thiemens. "Analytical procedure to determine both Δ^{18}O and Δ^{17}O of H_2O_2 in natural water and first measurements." Atmos. Env. 33: 3683-3690, 1996.

Sholkovitz, E. R., Sedwick, P. N., Church, T. M., Baker, A. R., and Powell, C. F.: Fractional solubility of aerosol iron: Synthesis of a global-scale data set, Geochimica et Cosmochimica Acta, 89, 173-189, 10.1016/j.gca.2012.04.022, 2012.

Solmon, F., Chuang, P. Y., Meskhidze, N., and Chen, Y.: Acidic processing of mineral dust iron by anthropogenic compounds over the north Pacific Ocean, J. Geophys.l Res., 114, doi:10.1029/2008jd010417, 2009.

Spokes, L. J., Jickells, T. D., and Lim, B.: Solubilisation of aerosol trace metals by cloud processing: A laboratory study, Geochimica et Cosmochimica Acta, 58, 3281-3287, doi:10.1016/0016-7037(94)90056-6, 1994.

Sun, Y. L., Wang, Z. F., Du, W., Zhang, Q., Wang, Q. Q., Fu, P. Q., Pan, X. L., Li, J., Jayne, J., and Worsnop, D. R.: Long-term real-time measurements of aerosol particle composition in Beijing, China: seasonal variations, meteorological effects, and source analysis, Atmos. Chem. Phys., 15, 10149-10165, doi:10.5194/acp-15-10149-2015, 2015.

Wang, H., Qiao, B., Zhang, L., Yang, F., and Jiang, X.: Characteristics and sources of trace elements in PM2.5 in two megacities in Sichuan Basin of southwest China, Environ. Pollut., 242, 1577-1586, doi:10.1016/j.envpol.2018.07.125, 2018.

Wang, Y., Jia, C., Tao, J., Zhang, L., Liang, X., Ma, J., Gao, H., Huang, T., and Zhang, K.: Chemical characterization and source apportionment of $PM_{2.5}$ in a semi-arid and petrochemical-industrialized city, Northwest China, Sci. Total Environ., 573, 1031-1040, doi:10.1016/j.scitotenv.2016.08.179, 2016.

Ye, C., Liu, P., Ma, Z., Xue, C., Zhang, C., Zhang, Y., Liu, J., Liu, C., Sun, X., and Mu, Y.: High H_2O_2 Concentrations Observed during Haze Periods during the Winter in Beijing: Importance of H_2O_2 Oxidation in Sulfate Formation, Environ. Sci. Technol. Lett., 5, 757-763, doi:10.1021/acs.estlett.8b00579, 2018.

Zhang, Y., Wen, L., Chen, J., Wang, X., Xue, L., Yang, L., Wang, L., Li, Z., Yu, C., Chen, T., and Wang, W.: Trend in Fine Sulfate Concentrations and the Associated Secondary Formation Processes at an Urban Site in North China, Aerosol and Air Quality Research, 18, 1519-1530, doi:10.4209/aaqr.2017.10.0358, 2018.

Zhao, P. S., Dong, F., He, D., Zhao, X. J., Zhang, X. L., Zhang, W. Z., Yao, Q., and Liu, H. Y.: Characteristics of concentrations and chemical compositions for $PM_{2.5}$ in the region of Beijing, Tianjin, and Hebei, China, Atmos. Chem. Phys., 13, 4631-4644, doi:10.5194/acp-13-4631-2013, 2013.